Sustainable Energy & Fuels

ROYAL SOCIETY OF CHEMISTRY

PAPER

View Article Online
View Journal | View Issue

Cite this: *Sustainable Energy Fuels*, 2022, **6**, 1983

A flexible self-poled piezocomposite nanogenerator based on $H_2(Zr_{0.1}Ti_{0.9})_3O_7$ nanowires and polylactic acid biopolymer†

Zouhair Hanani, *[abc] Ilyasse Izanzar,[a] Soukaina Merselmiz,[a] Taha El Assimi,[ad] Daoud Mezzane,[ae] M'barek Amjoud,[a] Hana Uršič,[c] Uroš Prah,[c] Jaafar Ghanbaja,[f] Ismael Saadoune,[ad] Mohammed Lahcini,[ad] Matjaž Spreitzer,[c] Damjan Vengust,[c] Mimoun El Marssi,[e] Zdravko Kutnjak,[c] Igor A. Luk'yanchuk[eg] and Mohamed Gouné[b]

The field of piezoelectric nanogenerators is rapidly growing as a promising technology for driving low-power portable devices and self-powered electronic systems by converting wasted mechanical energy into electric energy. In this study, we designed a flexible and self-poled piezocomposite nanogenerator based on lead-free $H_2(Zr_{0.1}Ti_{0.9})_3O_7$ (HZTO) nanowires and a polylactic acid (PLA) biodegradable polymer. By using a piezoresponse force microscope (PFM), the piezoelectric coefficient (d_{33}) of a single HZTO nanowire was found to be 26 pm V^{-1}. The piezoelectric energy harvesting performances of a self-poled piezocomposite film fabricated by embedding core–shell structured HZTO nanowires by polydopamine into the PLA matrix were tested. The piezoelectric nanogenerator demonstrated enhanced output performances (an open-circuit voltage of 5.41 V, short-circuit current of 0.26 μA and maximum power density of 463.5 μW cm^{-3} at a low resistive load of 2.5 MΩ). Besides, the developed device can charge different capacitors by regular mechanical impartations and can power a red light-emitting LED diode by various biomechanical motions. This study reveals the benefits of combining HZTO nanowires and PLA biopolymer in designing high-performance piezoelectric nanocomposites for biomechanical energy harvesting.

Received 21st February 2022
Accepted 8th March 2022

DOI: 10.1039/d2se00234e

rsc.li/sustainable-energy

1. Introduction

Now, the world is concerned about "green energy" and many researches are focusing on eco-friendly technologies for energy harvesting applications.[1–5] In this regard, the invention of piezoelectric nanogenerators (PNGs) by Wang *et al.* has opened a gate towards the mechanical energy harvesting of wasted energy in our environment.[6] Since then, piezoelectric nanogenerators (PNGs) are growing as a promising technology for harvesting mechanical energy into electricity through nanoscale piezoelectric materials.[7–10] However, the most used piezoelectric materials in the PNGs are lead-based, which raise environmental concerns.[8,11–13] The integration of lead-free materials is, therefore, essential.[14–18] Despite using lead-free ceramics in the ceramic-based PNGs, the mechanical flexibility, adaptability for large mechanical forces, manufacturing cost, and processing present new challenges.[19,20] Consequently, PNGs-based ceramic/polymer nanocomposites could be the best solution to overcome the above drawbacks.[21,22] However, majority of the studies on PNG-based ceramic/polymer nanocomposites relies on the use of polyvinylidene fluoride (PVDF) and polydimethylsiloxane (PDMS),[22–27] which are also problematic from the environmental point of view. Furthermore, composites based on given polymers are also incompatible for the *in vivo* incorporations of piezoelectric materials for biomedical applications. To address these issues, researchers are investigating the properties of biodegradable and renewable polymers and their integration into flexible, biocompatible and biodegradable electronics.[28–30]

Polylactic acid (PLA) is one of the most promising biopolymers in energy harvesting applications.[21,31–33] PLA is a biodegradable, biocompatible, non-toxic and ecological thermoplastic aliphatic polyester derived from a natural organic acid. PLA is becoming a popular candidate for energy harvesting applications owing to its high piezoelectric properties.[21,30,34,35] It is also worth noting

[a]*IMED-Lab, Cadi Ayyad University, Avenue Abdelkrim El Khattabi, P. B. 549, Marrakesh, 40000, Morocco*
[b]*ICMCB, University of Bordeaux, 87 Avenue du Dr Albert Schweitzer, Pessac, 33600, France*
[c]*Jozef Stefan Institute, Jamova Cesta 39, Ljubljana, 1000, Slovenia. E-mail: zouhair.hanani@ijs.si*
[d]*Mohammed VI Polytechnic University, Lot 660-Hay Moulay Rachid, Ben Guerir, 43150, Morocco*
[e]*LPMC, University of Picardy Jules Verne, 33 Rue Saint Leu, Amiens, 80039, France*
[f]*IJL, University of Lorraine, 54000, Nancy, France*
[g]*Department of Building Materials, Kyiv National University of Construction and Architecture, Kyiv, 03680, Ukraine*

† Electronic supplementary information (ESI) available. See DOI: 10.1039/d2se00234e

that contrary to the majority of PNGs based on PVDF or PDMS, which require a poling process to promote piezoelectric activity, the carbonyl groups branching out from the PLA backbone induce polarity, thus exhibiting a $d_{14} \sim 10$ pC N^{-1} without any additional poling step.[21,30,36] The self-polarization was reported to be an amazing technique to eliminate the complexity of the traditional electrical poling process for piezoelectric and ferroelectric material-based energy harvesting devices.[37] For instance, in PVDF, this could be reached by stabilising the electroactive β-phase by embedding piezoelectric fillers.[38,39]

To enhance the PNG electrical performances, considerable attention has been focused on 1D nanomaterials due to their improved electrical properties.[40–42] Particularly, embedding 1D nanofillers into the polymer matrix could improve the electrical outputs at a low concentration due to the enhancement of local fields, which is beneficial for decreasing the surface energy and alleviating the agglomeration of the nanofillers in the polymeric matrixes.[43,44]

In this regard, $H_2Ti_3O_7$ (HTO) biocompatible nanowires are a promising material for energy storage and harvesting applications.[45–47] HTO nanowires easily undergo ion-exchange reaction and conversion *via* a simple hydrothermal method into 1D-perovskite oxides, such as $BaTiO_3$, primarily used in energy storage and energy harvesting applications.[48–50] In particular, Zr-doped HTO nanowires ($H_2(Zr_yTi_{1-y})_3O_7$, HZTO) are used to fabricate 1D-perovskite oxides with fascinated ferroelectric and piezoelectric properties similar to the state-of-the-art $PbZr_yTi_{1-y}O_3$ (PZT) and $Ba_{1-x}Ca_xZr_yTi_{1-y}O_3$ (BCZT).[51–54] Nevertheless, to the best of our knowledge, the piezoelectric properties and mechanical energy harvesting capability of HZTO nanowires have not yet been investigated.

In this study, the piezoelectric response of HZTO-nws was investigated by a piezoresponse force microscope (PFM). The piezoelectric coefficient d_{33} of HZTO nanowires was found to be 26 pm V^{-1}. HZTO-nws were core–shell structured by polydopamine (PDA) to facilitate their dispersion into the PLA matrix.[7,55,56] The energy harvesting ability of HZTO nanowires was explored by designing a flexible piezocomposite nanogenerator (nw-PNG) based on surface-modified HZTO nanowires and PLA biopolymer. The as-prepared nw-PNG exhibited enhanced output performances (open-circuit voltage of 5.41 V and short-circuit current of 0.26 μA) and could drive small commercial electronics (charging a capacitor and glowing a red light-emitting diode under various human motions).

2. Experimental section

2.1 Materials

Polylactic acid (PLA), with reference Ingeo™ Biopolymer 6201D, was purchased from NatureWorks. Sodium hydroxide (≥97.0%), hydrogen peroxide solution (30% wt in H_2O), Tris–HCl (≥99.0%), ethanol (96%), dichloromethane (≥99.9%), and hydrochloric acid (37%) were purchased from Sigma Aldrich, while dopamine hydrochloride (99%) was obtained from Alfa Aesar. Demineralized water with a resistivity of 18.2 MΩ cm^{-1} was obtained from a PURELAB-classic water purification system (ELGA LabWater) and was used during the experiments conducted in this study. A commercially available Cu foil (>99.99%, 9 μm thickness) was obtained from MTI corporation.

2.2 Preparation of HZTO nanowires

To prepare $H_2(Zr_{0.1}Ti_{0.9})_3O_7$ nanowires (HZTO-nw), 5 g of $Zr_{0.1}Ti_{0.9}O_2$ (ZTO) powder, synthesized as described elsewhere,[57] was dispersed in 100 mL of 10 M NaOH aqueous solution. After 1 h of stirring, the suspension was transferred to a 150 mL-Teflon-lined stainless-steel autoclave, sealed and heated to 240 °C with 48 h dwell time, followed by cooling down to room temperature. The resulting white suspension of $Na_2(Zr_{0.1}Ti_{0.9})_3O_7$ (NaZTO) was collected by filtration and soaked in 0.2 M HCl solution for 10 h to convert NaZTO to HZTO. The latter was washed several times with deionized water and ethanol *via* repeated centrifugation at 4000 rpm for 10 min until reaching the neutrality of the medium (pH = 7). The filtered HZTO-nw were redispersed in deionized water by mechanical stirring at 60 rpm for 30 min, and then freeze-dried for 48 h to obtain a fluffy product.

2.3 Core–shell structuration of HZTO nanowires

To promote the chemical interactions between HZTO-nw and PLA biopolymer, the surface of the HZTO nanowires was first hydroxyled and then coated with a polydopamine (PDA) shell. HZTO nanowires were first dispersed in a hydrogen peroxide solution (H_2O_2) using ultrasound for 30 min and then refluxed at 104 °C for 4 h. The obtained hydroxylated product (HZTO-nw-OH) was recovered by centrifugation at 12 000 rpm for 10 min, washed several times with demineralized water and ethanol and then dried under vacuum at 80 °C for 12 h. Subsequently, the hydroxylated HZTO nanowires were coated with a PDA shell by the air oxidation of dopamine to form HZTO-nw@PDA. For that purpose, 1 g of the HZTO-nw-OH powder was dispersed in 100 mL of the Tris–HCl (0.01 M) by applying ultrasound for 10 min. The pH of the aqueous dopamine solution was buffered to 8.5 by adding the 0.01 M Tris–HCl. After 24 h of reaction at reflux at 60 °C, a black powder HZTO-nw@PDA was recovered by centrifugation at 12 000 rpm for 10 min, washed several times with demineralized water and ethanol, and then dried at 80 °C for 24 h.

2.4 Elaboration of PLA-based nanocomposite films

HZTO-nw@PDA/PLA nanocomposite films were elaborated by the solution casting method using 0, 5, 10, 20 and 30 vol% of HZTO-nw@PDA fillers. Explicitly, an adequate amount of PLA was solubilized in dichloromethane under magnetic stirring for 2 h. Subsequently, HZTO-nw@PDA nanowires were dispersed therein by ultrasound for 15 min, and then homogenized by magnetic stirring for another 2 h. The slurry was cast in a Teflon Petri dish and dried at room temperature to obtain a flexible composite film, and then dried in a vacuum at 40 °C for 12 h to remove the solvent.

2.5 Fabrication of the nw-PNG device

PLA-based piezocomposites using 0, 5, 10, 20 and 30 vol% HZTO-nw@PDA (nw-PNG) were sandwiched between two copper foils of 3.0 × 1.5 cm^2 serving as top and bottom

electrodes. For external connections, two copper wires were welded to the upper and bottom electrodes to measure the electrical outputs. Then, the nw-PNG were additionally encapsulated by using the Kapton tape. This encapsulation prevented damage of the nw-PNG by repeated mechanical excitations and made it water- and dustproof.

2.6 Characterisations

The morphological properties of HZTO-nw and the 20 vol% HZTO-nw@PDA/PLA nanocomposite film were analysed using a field-emission scanning electron microscope (FESEM, JEOL JSM-7600F). A transmission electron microscope (JEOL – ARM 200F Cold FEG TEM/STEM) equipped with an energy-dispersive X-ray (EDX) spectrometer was used to visualize the HZTO nanowire morphology, *i.e.*, to test the success of the core–shell structuration with PDA, and to probe the HZTO nanowire composition. A Discovery Series TGA 55 (TA instruments) device was used to characterize the thermal evolution of HZTO-nw, HZTO-nw@PDA, PLA and 20 vol% HZTO-nw@PDA/PLA from room temperature to 600 °C at a heating rate of 10 °C min^{-1} in a nitrogen flow of 40 mL min^{-1}. The local piezoelectric responses of HZTO nanowires were investigated on an atomic force microscope (AFM, Asylum Research, MFP-3D) equipped with a piezo-response force module (PFM). A Ti/Ir-coated Si tip with a ~20 nm radius of curvature (Asyelec, Atomic Force F&E GmbH) was used. To avoid sticking the HZTO nanowire to the PFM tip and moving them during scanning, the nanowires were fixed *via* a thermal treatment (heating to 700 °C for 1 h in O_2).[58] The HZTO-nw were deposited on a Pt-conductive substrate serving as a bottom electrode, and the measurements were made in the regular ground regime to extract the d_{33} values. The local piezoelectric values were determined in a PFM single frequency mode by applying an AC voltage with an amplitude of 12 V and a frequency of 318 kHz (more than 30 kHz away from contact resonance frequency). The local piezoelectric response d_{33} was determined by dividing the maximum amplitude value (obtained by the program Gwyddion 2.41) with amplitude of the applied voltage, *i.e.*, 12 V. The average thickness of the nanocomposite film was measured by a precise coating thickness gauge (Surfix Pro S, Phynix). To study the flexible piezocomposite nanogenerator (nw-PNG) output performances, the open-circuit voltage and short-circuit current were measured using a potentiostat (SP-150, Bio-Logic). The approximate contact force of finger tapping, 2 N, was evaluated experimentally by using a dual column mechanical testing system (Instron, 3369). All measurements were carried out at room temperature.

3. Results and discussions

3.1 Structural and piezoelectric properties of HZTO nanowires

Fig. 1 presents the XRD pattern and FESEM image of HZTO nanowires. All XRD peaks can be indexed to monoclinic symmetry (JCPDS 41-0192) with the *C*2/*m* space group; however, only the most intense peaks are assigned (Fig. 1a).[45,46,54,59] A typical TEM image of the HZTO-nw is shown in the inset of Fig. 1a. The corresponding selected area electron diffraction (SAED) (inset Fig. 1a) indicates that the sample shows a well-crystallized one-dimensional morphology. The SAED is indexed to the monoclinic *C*2/*m* space group. The lattice

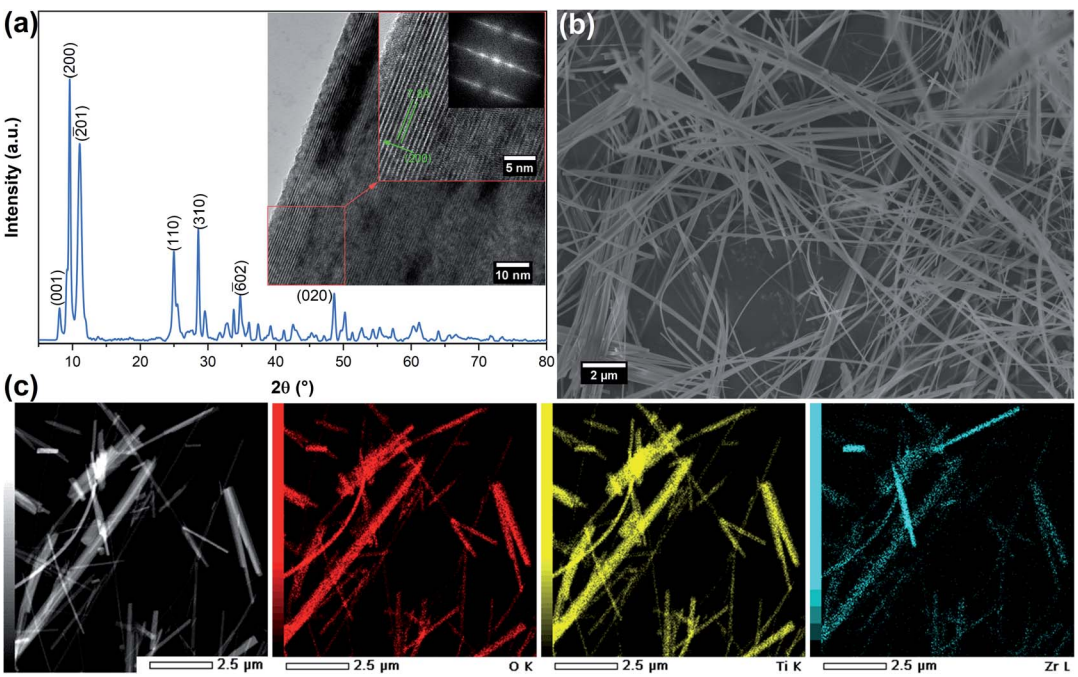

Fig. 1 (a) XRD pattern of HZTO nanowires' powder (insets show TEM image and SAED pattern), (b) FESEM image of HZTO nanowires, and (c) STEM image and EDX elemental mapping images of HZTO nanowires. The red, yellow, and blue areas correspond to O, Ti, and Zr elements, respectively.

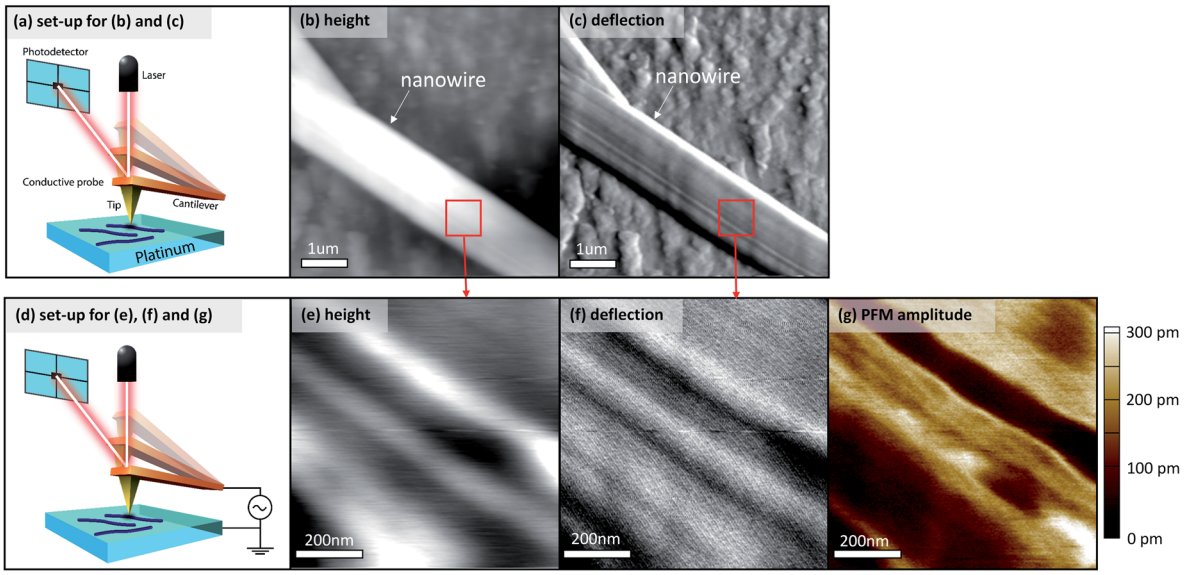

Fig. 2 (a) Scheme of experimental set-up for AFM topography measurements shown in panels (b) height and (c) deflection. (d) Scheme of experimental set-up for PFM measurements shown in panels (e) height, (f) deflection and (g) out-of-plane PFM amplitude measurements of a single HZTO-nw.

spacing of 7.8 Å corresponds to the reticular distance of the (200) diffraction peak of the monoclinic $H_2Ti_3O_7$ crystal. Moreover, Fig. 1b shows the free-standing HZTO nanowires with a high aspect ratio of around 50. This high aspect ratio is due to the relatively high reaction temperature (240 °C) and/or prolonged reaction time (48 h).[49] Besides, Fig. 1c presents the STEM image and EDX elemental mapping images of HZTO-nw proving the presence and the homogeneous distribution of O, Ti and Zr elements.

The local piezoelectric response of HZTO nanowires was investigated by PFM. In the first step, only a classic AFM topography analysis was performed (no electric field applied) to locate the nanowires for the piezo-response analysis (Fig. 2a–c). After the finding the location using AFM examination, the electric field was applied between the conductive AFM tip and the bottom electrode (Pt-substrate), as illustrated in Fig. 2d, and the scan was performed only on the top of the chosen nanowire to avoid electrical short circuit. In Fig. 2g, the PFM out-of-plane amplitude response is shown. Compared to the darker areas, the brightest areas correspond to an enhanced local piezoelectric activity. The maximum local piezoelectric response d_{33} value reached 26 pm V^{-1}. This value is comparable to that (28 pm V^{-1}) measured in bowl-like $BaTiO_3$ particles,[60] higher than that reported in $BaTiO_3$ nanofibers (20 pm V^{-1}),[61,62] $Ba_{1-x}Sr_x$-TiO_3 plates (20 pm V^{-1}),[58] and lower than that stated by Zhuang *et al.* in $BaTiO_3$ Ce-doped nanofibers (42 pm V^{-1}).[63]

3.2 Energy harvesting performances of PNG-based HZTO nanowires

To check the energy harvesting capability of HZTO nanowires, a flexible piezocomposite nanogenerator (nw-PNG) based on HZTO-nw and PLA biopolymer was designed. In order to facilitate their dispersion into the PLA matrix, HZTO-nw were core–

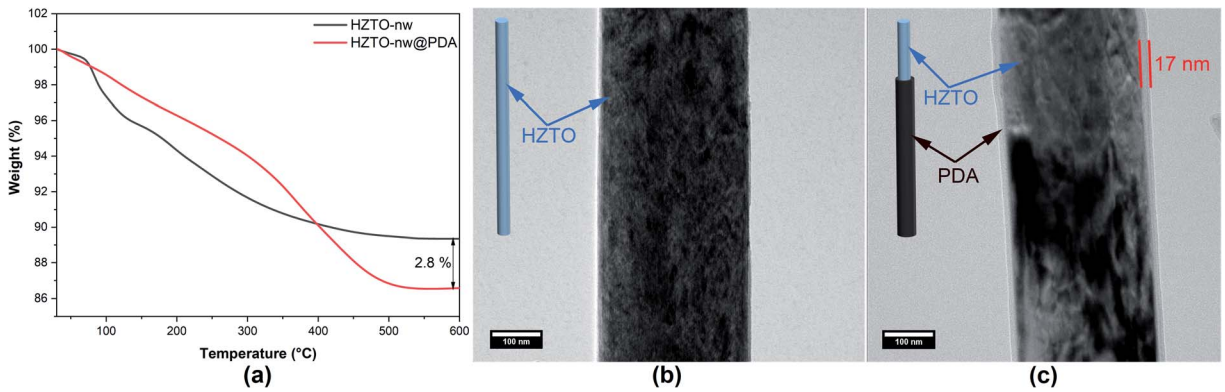

Fig. 3 Results of the successful core–shell structuring of HZTO nanowires using PDA. (a) TGA curves of pure HZTO-nw and HZTO-nw@PDA. TEM micrographs of (b) HZTO-nw and (c) HZTO-nw@PDA. Insets schematically represent the observed morphologies.

shell structured by polydopamine (PDA) to obtain HZTO-nw@PDA. Thermogravimetric analysis (TGA) was employed to investigate the thermal stability between the pristine and surface modified nanowires. As shown in Fig. 3a, the total weight losses of the pristine HZTO-nw and HZTO-nw@PDA from 30 °C to 600 °C were about 10.64 wt% and 13.44 wt%, respectively. The increase in weight loss after functionalization can be attributed to the presence of the PDA layer on the HZTO nanowire surface (Fig. 3b and c), where a PDA shell of about 17 nm was coated on the HZTO surface. PDA deposition gave a distinct thin layer on the nanowire surface, which facilitates the dispersion of nanowires in the polymer matrix.

The surface and cross-section morphological properties of the 20 vol% HZTO-nw@PDA/PLA nanocomposite film are presented in Fig. 4a and b. A dense nanocomposite film with 40 μm thickness with uniformly distributed nanowires can be observed. The black regions correspond to the PLA matrix, and the white spots represent the HZTO-nw@PDA filler. It is clearly seen that HZTO-nw@PDA nanowires are evenly embedded in the PLA polymer matrix, indicating the excellent compatibility between PLA and fillers. The flexibility of the as-prepared nanocomposite film is demonstrated in the inset of Fig. 4a.

To evaluate the ability of the elaborated piezocomposite films for harvesting biomechanical energy, piezoelectric nanogenerators with different HZTO-nw@PDA concentrations (0, 5, 10, 20 and 30 vol%) were designed. Fig. 4c and d depict a photograph and schematic of the designed flexible piezocomposite nanogenerator device using 20 vol% HZTO-nw@PDA. To gain insights on the effects of the HZTO-nw@PDA concentration on the piezoelectric performances, specifically the open circuit voltage (V_{oc}), the fabricated nanogenerators were subjected to finger impartations of 2 N, and the resulting V_{oc} were recorded and presented in Fig. S1 in the ESI.† It was observed that the output voltage was amplified significantly with the increase in HZTO-nw@PDA concentration. This can be explained by an enhancement of the dielectric constant of the composite with nanofiller addition. A higher dielectric constant of nanocomposite films has a good capability of storage charge, which can lead to better piezoelectric properties.[64] Nevertheless, excessive HZTO-nw@PDA content will cause the agglomeration and deterioration of the mechanical properties, limits the movement of PLA dipoles and eventually weakens the polarizability of the nanocomposite, which results in a decline of the piezoelectric performance.[65] Accordingly, we will focus only on the piezocomposite with 20 vol% of HZTO-nw@PDA.

Fig. 4e and f illustrate the open-circuit voltage (V_{oc}) and short-circuit current (I_{sc}) of 20 vol% HZTO-nw@PDA/PLA (nw-PNG) under finger impartations. The nw-PNG can produce V_{oc} and I_{sc} of 5.41 V and 0.26 μA, respectively. The averaged peak-to-peak V_{oc} and I_{sc} are 7.8 V and 0.4 μA, respectively. The slight variation in the amplitude of each pulse could be attributed to the manual stress variation during the finger tapping sequence. Interestingly, the obtained electrical outputs are superior to some previous PDMS or PVDF composite-based PNG without any prior electrical poling process.[66–71] As shown before, this can be ascribed to the natural piezoelectricity developed in PLA after mechanical stress application and the surface-charge induced polarization.[21,72,73]

To verify the purity of the piezoelectric effect in the nw-PNG device under pressing and releasing motions, the switching polarity test was conducted.[74] As presented in Fig. S2 in the

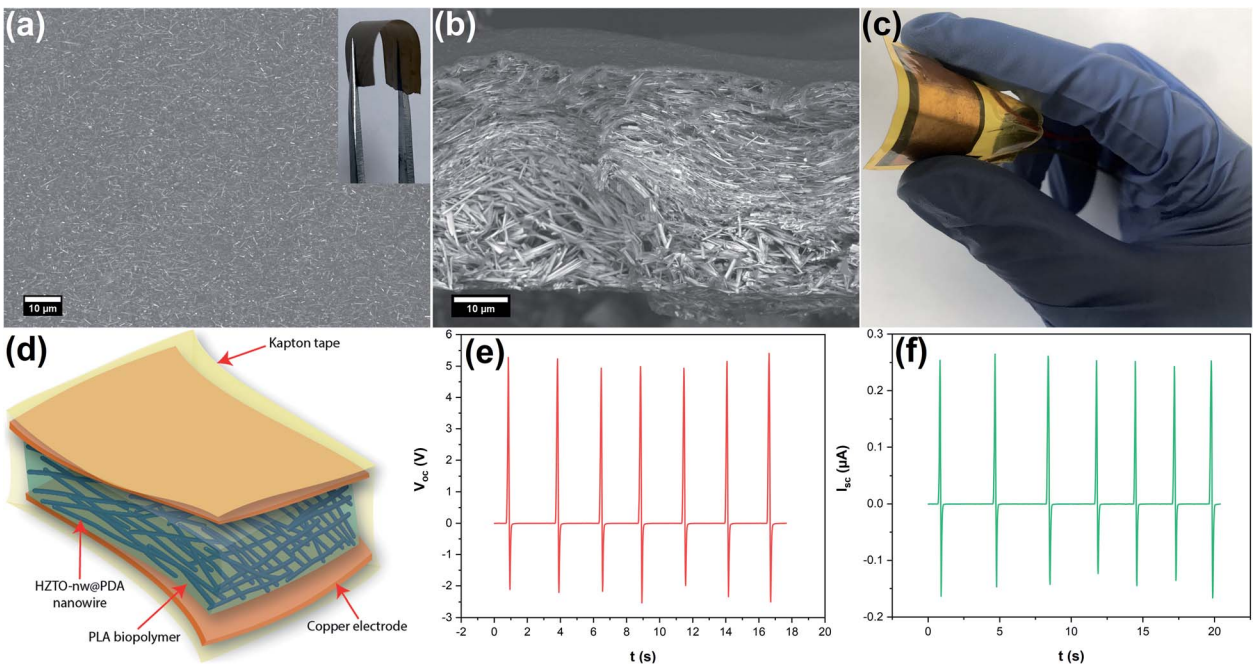

Fig. 4 FESEM images of the (a) surface (inset shows a photograph illustrating the flexibility of the nanocomposite film) and (b) cross-section of the HZTO-nw@PDA/PLA nanocomposite film. (c) Photograph and (d) schematic illustration of the fabricated piezocomposite nanogenerator device. The generated (e) open-circuit voltage and (f) short-circuit current under finger tapping.

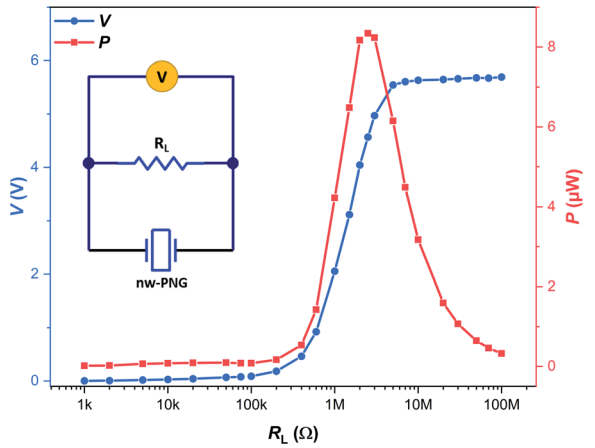

Fig. 5 The output voltage and power density generated by the nw-PNG across various resistors (inset shows the schematic circuit diagram of the harvested output voltage).

ESI,† when the nw-PNG device is forward-connected to the measurement kit, upward output signals followed by downward output signals are obtained. In contrast, the signal direction is inverted in the reverse connection. The observation of such signal output switching by changing the polarity confirms that the energy harvesting signals are the product of piezoelectricity from the flexible nw-PNG device.[75]

The suggested working mechanism of the nw-PNG nanogenerator can be explained in terms of the combined/synergistic effect of the PLA dipoles and high surface charge on HZTO-nw@PDA. The β-phase of PLA has flexible molecular chains containing C=O dipoles, where the crystal structure is characterized by the helical structure and the shear piezoelectricity at the molecular level originating from the dipole accompanies the asymmetric carbon.[76] When the shear strain induced by the electric field is applied to the molecular chain of the PLA through its side chain, the displacement arises in all the atoms. The motions causing a change in polarization is the rotation of the plane defined by the C–O and C=O bond on the C–O bond of PLA, which was reported as perpendicular to the electric field. Accordingly, the change in polarization arises due to the applied stress.[36]

Compared to PVDF or other piezoceramics, PLA-based piezoelectric materials own lower piezo-responses.[76] Accordingly, embedding piezoelectric fillers into the PLA matrix could be beneficial by increasing the portion of the desirable electroactive β-phase, thus enhancing the piezoelectric properties.[77] In our case, the presence of an oppositely charged polar surface on HZTO-nw@PDA aggressively interacts with the different C=O dipoles of PLA, resulting in the development of negative and positive charge densities over the nanocomposite surface, which promotes the formation of piezoelectric polar β-phase through surface charge-induced polarization. Besides, the applied mechanical strain induces a potential in HZTO-nw@PDA, which additionally aligned the C=O dipoles in the direction of applied force through stress induced polarization.[38]

The self-poling aspect in nw-PNG results from some degree of molecular alignment of the PLA chains along the length of the HZTO-nw@PDA. Alternatively, the PLA molecules are self-polarised in a favourable direction by the dual effect of stress and surface charge-induced polarization without applying any external electric field. Accordingly, the use of the PLA biopolymer could eliminate the complexity of the traditional electrical poling process in the piezoelectric energy harvesters.

For real-time applications, the device cannot operate in an open circuit, instead must be connected to external loads (R_L).[78] The energy performance of the nw-PNG was examined by measuring the output voltage characteristic at various external resistive loads (inset of Fig. 5). The output voltage increases with the increase in the load resistance, while the power density ($P = V^2/R_L$) increased first to reach a maximal value $P_{max} = 8.4$ μW at

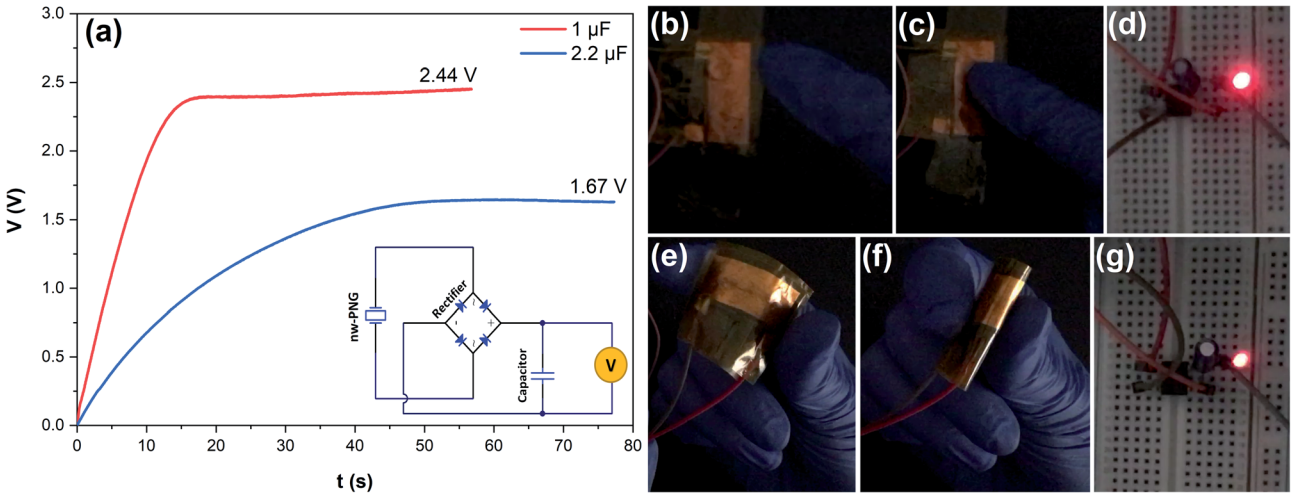

Fig. 6 The test results for the feasibility of the fabricated nw-PNG device. (a) The charging curves of 1 μF and 2.2 μF-capacitors using the piezocomposite nanogenerator under sewing machine impartations (the inset shows the electrical circuit diagram used to harvest the electric energy from the nw-PNG device). Photographic images of the process of the red LED glowing (b–d) under finger tapping and (e–g) under folding/unfolding motions using the nw-PNG.

$R_L = 2.5$ MΩ, and then decreased with an increase in R_L. The corresponding area and volumetric power densities are $P^s_{max} = 1.85$ μW cm^{-2} and $P^v_{max} = 463.5$ μW cm^{-3}, respectively. These values are enhanced compared to some reported piezoelectric nanogenerators.[11,41,42,69,70,79]

The feasibility of the nw-PNG as a powering device for small portable electronics was demonstrated by integrating the nw-PNG into electrical circuits to charge different capacitors and to power a red light-emitting diode (LED). To charge the discharged capacitors, a sewing machine was used as a constant stress and frequency source. In this test, the sewing machine needle was substituted by a cylindrical plastic piece with a tapping area close to a human finger, as described in our previous study.[7] The nw-PNG device was used to charge 1 μF and 2.2 μF capacitors under sewing machine impartations at a frequency of 23 Hz, as shown in Fig. 6a. The inset of Fig. 6a shows the schematic circuit diagram used to track the accumulated voltage across the capacitor upon charge. The circuit includes a full-wave bridge rectifier, a capacitor, and a piezoelectric device. The nw-PNG can charge the 1 μF and 2.2 μF capacitors up to 2.44 and 1.67 V, respectively, which correspond, according to $U_e = 1/2CV^2$, to the stored energies of 2.97 and 3.07 μJ and equivalent energy densities of 0.16 and 0.17 mJ cm^{-3}, respectively. Here, U_e, C, and V denote the stored electric density, capacitor capacity, and generated voltage, respectively. Furthermore, the nw-PNG was also employed to light up a red LED with finger tapping (Fig. 6b–d and Video S1 in the ESI†) and folding/unfolding motions (Fig. 6e–g and Video S2 in the ESI†), using the schematic circuit diagram of Fig. S3 in the ESI.† Our flexible and self-poled piezocomposite device can efficiently drive a red LED under different human motions without any noticeable degradation. Because we used nontoxic chemicals, we can easily imagine its integration as self-powered electronics in the biomedical field.

4. Conclusions

A flexible piezocomposite nanogenerator (nw-PNG) based on lead-free core–shell structured HZTO nanowires and PLA biopolymer was designed. The local piezoelectricity of HZTO-nw was investigated on a piezoresponse force microscope, and the piezoelectric coefficient of a single HZTO nanowire was found to be 26 pm V^{-1}. This value is higher compared to the $BaTiO_3$ nanofibers (20 pm V^{-1}). The fabricated nw-PNG exhibited enhanced output performances ($V_{oc} = 5.41$ V, $I_{sc} = 0.26$ μA and $P^v_{max} = 463.5$ μW cm^{-3} at $R_L = 2.5$ MΩ) and has demonstrated its ability to drive capacitors with different capacitances under sewing machine impartations, and a red LED under different human motions. The as-prepared piezocomposite nanogenerator could be easily integrated into self-powered electronics in biomedical applications, such as monitoring human health conditions.

Author contributions

Zouhair Hanani: conceptualization, formal analysis, investigation, data curation, methodology, writing – original draft. Ilyasse Izanzar: conceptualization, investigation, data curation, methodology. Soukaina Merselmiz: conceptualization, data curation, visualization. Taha El Assimi: methodology, investigation, data curation. Daoud Mezzane: supervision, project administration, funding acquisition. M'barek Amjoud: supervision. Hana Uršič: resources, investigation, writing – review & editing, validation. Uroš Prah: writing – review & editing, validation. Jaafar Ghanbaja: resources, investigation. Ismael Saadoune: resources, writing – review & editing. Mohammed Lahcini: supervision, resources, writing – review & editing. Matjaž Spreitzer: resources, funding acquisition, writing – review & editing, validation. Damjan Vengust: investigation, data curation, writing – review & editing. Mimoun El Marssi: project administration, funding acquisition. Zdravko Kutnjak: project administration, resources, validation, funding acquisition, writing – review & editing. Igor A. Luk'yanchuk: project administration, validation, funding acquisition, writing – review & editing. Mohamed Gouné: supervision, project administration.

Conflicts of interest

There are no conflicts to declare.

Acknowledgements

The authors gratefully acknowledge the generous financial support of the European Union Horizon 2020 Research and Innovation actions MSCA-RISE-ENGIMA (No. 778072) and MSCA-RISE-MELON (No. 872631). Z. K., M. S., H. U. and U. P. acknowledge the Slovenian Research Agency programs P1-0125, P2-0091 and P2-0105. H. U. thanks Jena Cilenšek and Mateo Milicevic (Erasmus+ program) for help in the laboratory.

References

1 B. A. Bhanvase and V. B. Pawade, *Nanomaterials for Green Energy*, Elsevier, 2018, pp. 457–472.
2 S. A. Han, J. Lee, J. Lin, S. W. Kim and J. H. Kim, *Nano Energy*, 2019, **57**, 680–691.
3 B. Chen, Y. Yang and Z. L. Wang, *Adv. Energy Mater.*, 2018, **8**, 1702649.
4 Z. Hanani, S. Merselmiz, D. Mezzane, M. Amjoud, A. Bradeško, B. Rožič, M. Lahcini, M. El Marssi, A. V. Ragulya, I. A. LukYanchuk, Z. Kutnjak and M. Gouné, *RSC Adv.*, 2020, **10**, 30746–30755.
5 S. Merselmiz, Z. Hanani, U. Prah, D. Mezzane, L. Hajji, Z. Abkhar, M. Spreitzer, D. Vengust, H. Uršič, D. Fabijan, A. G. Razumnaya, O. Shapovalova, I. A. Lukyanchuk and Z. Kutnjak, *Phys. Chem. Chem. Phys.*, 2022, **24**(10), 6026–6036.
6 Z. L. Wang and J. Song, *Science*, 2006, **312**, 242–246.
7 Z. Hanani, I. Izanzar, M. Amjoud, D. Mezzane, M. Lahcini, H. Uršič, U. Prah, I. Saadoune, M. El Marssi, I. A. Lukyanchuk, Z. Kutnjak and M. Gouné, *Nano Energy*, 2021, **81**, 105661.

8 S. K. Si, S. K. Karan, S. Paria, A. Maitra, A. K. Das, R. Bera, A. Bera, L. Halder and B. B. Khatua, *Mater. Chem. Phys.*, 2018, **213**, 525–537.
9 N. R. Alluri, A. Chandrasekhar, V. Vivekananthan, Y. Purusothaman, S. Selvarajan, J. H. Jeong and S. J. Kim, *ACS Sustainable Chem. Eng.*, 2017, **5**, 4730–4738.
10 Y. Zhang, H. Kim, Q. Wang, W. Jo, A. I. Kingon, S. H. Kim and C. K. Jeong, *Nanoscale Adv.*, 2020, **2**, 3131–3149.
11 X. Niu, W. Jia, S. Qian, J. Zhu, J. Zhang, X. Hou, J. Mu, W. Geng, J. Cho, J. He and X. Chou, *ACS Sustainable Chem. Eng.*, 2019, **7**, 979–985.
12 K. Il Park, J. H. Son, G. T. Hwang, C. K. Jeong, J. Ryu, M. Koo, I. Choi, S. H. Lee, M. Byun, Z. L. Wang and K. J. Lee, *Adv. Mater.*, 2014, **26**, 2514–2520.
13 G. T. Hwang, H. Park, J. H. Lee, S. Oh, K. Il Park, M. Byun, H. Park, G. Ahn, C. K. Jeong, K. No, H. Kwon, S. G. Lee, B. Joung and K. J. Lee, *Adv. Mater.*, 2014, **26**, 4880–4887.
14 P. K. Panda and B. Sahoo, *Ferroelectrics*, 2015, **474**, 128–143.
15 S. Merselmiz, Z. Hanani, S. Ben Moumen, A. Matavž, D. Mezzane, N. Novak, Z. Abkhar, L. Hajji, M. Amjoud, Y. Gagou, K. Hoummada, D. Črešnar, Z. Kutnjak and B. Rožič, *J. Mater. Sci.: Mater. Electron.*, 2020, **31**, 17018–17028.
16 S. Merselmiz, Z. Hanani, D. Mezzane, A. G. Razumnaya, M. Amjoud, L. Hajji, S. Terenchuk, B. Rožič, I. A. Lukyanchuk and Z. Kutnjak, *RSC Adv.*, 2021, **11**, 9459–9468.
17 Z. Hanani, D. Mezzane, M. Amjoud, Y. Gagou, K. Hoummada, C. Perrin, A. G. Razumnaya, Z. Kutnjak, A. Bouzina, M. El Marssi, M. Gouné and B. Rožič, *J. Mater. Sci.: Mater. Electron.*, 2020, **31**, 10096–10104.
18 Z. Hanani, D. Mezzane, M. Amjoud, A. G. Razumnaya, S. Fourcade, Y. Gagou, K. Hoummada, M. El Marssi and M. Gouné, *J. Mater. Sci.: Mater. Electron.*, 2019, **30**, 6430–6438.
19 S. K. Karan, S. Maiti, J. H. Lee, Y. K. Mishra, B. B. Khatua and J. K. Kim, *Adv. Funct. Mater.*, 2020, **30**, 2004446.
20 C. Baek, J. E. Wang, S. Ryu, J. H. Kim, C. K. Jeong, K. Il Park and D. K. Kim, *RSC Adv.*, 2017, **7**, 2851–2856.
21 S. Mishra, L. Unnikrishnan, S. K. Nayak and S. Mohanty, *Macromol. Mater. Eng.*, 2019, **304**, 1800463.
22 D. Hu, M. Yao, Y. Fan, C. Ma, M. Fan and M. Liu, *Nano Energy*, 2019, **55**, 288–304.
23 M. A. Parvez Mahmud, N. Huda, S. H. Farjana, M. Asadnia and C. Lang, *Adv. Energy Mater.*, 2018, **8**, 1–25.
24 Y. Zhang, M. Wu, Q. Zhu, F. Wang, H. Su, H. Li, C. Diao, H. Zheng, Y. Wu and Z. L. Wang, *Adv. Funct. Mater.*, 2019, **29**, 1904259.
25 Z. Zhou, Z. Zhang, Q. Zhang, H. Yang, Y. Zhu, Y. Wang and L. Chen, *ACS Appl. Mater. Interfaces*, 2020, **12**, 1567–1576.
26 E. L. Tsege, G. H. Kim, V. Annapureddy, B. Kim, H. K. Kim and Y. H. Hwang, *RSC Adv.*, 2016, **6**, 81426–81435.
27 G. Jian, Y. Jiao, Q. Meng, H. Shao, F. Wang and Z. Wei, *Adv. Mater. Interfaces*, 2020, **7**, 2000484.
28 X. Zeng, L. Deng, Y. Yao, R. Sun, J. Xu and C. P. Wong, *J. Mater. Chem. C*, 2016, **4**, 6037–6044.
29 D. Ponnamma, K. K. Sadasivuni and M. A. AlMaadeed, *Introduction of Biopolymer Composites: what to Do in Electronics?*, 2017.
30 X. Li, S. Chen, X. Zhang, J. Li, H. Liu, N. Han and X. Zhang, *Energy Technol.*, 2020, **8**, 1901252.
31 M. Smith, Y. Calahorra, Q. Jing and S. Kar-Narayan, *APL Mater.*, 2017, **5**, 074105.
32 S. Gong, B. Zhang, J. Zhang, Z. L. Wang and K. Ren, *Adv. Funct. Mater.*, 2020, **30**, 1908724.
33 E. J. Curry, K. Ke, M. T. Chorsi, K. S. Wrobel, A. N. Miller, A. Patel, I. Kim, J. Feng, L. Yue, Q. Wu, C. L. Kuo, K. W. H. Lo, C. T. Laurencin, H. Ilies, P. K. Purohit and T. D. Nguyen, *Proc. Natl. Acad. Sci. U. S. A.*, 2018, **115**, 909–914.
34 M. Varga, J. Morvan, N. Diorio, E. Buyuktanir, J. Harden, J. L. West and A. Jákli, *Appl. Phys. Lett.*, 2013, **102**, 153903.
35 M. Ando, S. Takeshima, Y. Ishiura, K. Ando and O. Onishi, *Jpn. J. Appl. Phys.*, 2017, **56**, 10PG01.
36 V. Sencadas, C. Ribeiro, A. Heredia, I. K. Bdikin, A. L. Kholkin and S. Lanceros-Mendez, *Appl. Phys. A: Mater. Sci. Process.*, 2012, **109**, 51–55.
37 R. A. Whiter, V. Narayan and S. Kar-Narayan, *Adv. Energy Mater.*, 2014, **4**, 1400519.
38 S. K. Karan, R. Bera, S. Paria, A. K. Das, S. Maiti, A. Maitra and B. B. Khatua, *Adv. Energy Mater.*, 2016, **6**, 1601016.
39 P. Thakur, A. Kool, N. A. Hoque, B. Bagchi, F. Khatun, P. Biswas, D. Brahma, S. Roy, S. Banerjee and S. Das, *Nano Energy*, 2018, **44**, 456–467.
40 X. Ni, F. Wang, A. Lin, Q. Xu, Z. Yang and Y. Qin, *Sci. Adv. Mater.*, 2013, **5**, 1781–1787.
41 M. R. Joung, H. Xu, I. T. Seo, D. H. Kim, J. Hur, S. Nahm, C. Y. Kang, S. J. Yoon and H. M. Park, *J. Mater. Chem. A*, 2014, **2**, 18547–18553.
42 W. Wu, S. Bai, M. Yuan, Y. Qin, Z. L. Wang and T. Jing, *ACS Nano*, 2012, **6**, 6231–6235.
43 S. Pradhan, R. Lach, H. H. Le, W. Grellmann, H.-J. Radusch and R. Adhikari, *ISRN Polym. Sci.*, 2013, **2013**, 1–9.
44 Z. Pan, L. Yao, G. Ge, B. Shen and J. Zhai, *J. Mater. Chem. A*, 2018, **6**, 14614–14622.
45 M. Zarrabeitia, E. Castillo-Martínez, J. M. López Del Amo, A. Eguía-Barrio, M. A. Muñoz-Márquez, T. Rojo and M. Casas-Cabanas, *J. Power Sources*, 2016, **324**, 378–387.
46 K. Kataoka, N. Kijima and J. Akimoto, *Inorg. Chem.*, 2013, **52**, 13861–13864.
47 D. K. Lee, I. S. Cho, S. W. Lee, D. H. Kim, H. W. Shim, D. W. Kim and K. S. Hong, *Eur. J. Inorg. Chem.*, 2010, **2010**, 1343–1347.
48 N. Bao, L. Shen, G. Srinivasan, K. Yanagisawa and A. Gupta, *J. Phys. Chem. C*, 2008, **112**, 8634–8642.
49 H. Tang, Z. Zhou and H. A. Sodano, *ACS Appl. Mater. Interfaces*, 2014, **6**, 5450–5455.
50 Y. Lin, D. Li, M. Zhang, S. Zhan, Y. Yang, H. Yang and Q. Yuan, *ACS Appl. Mater. Interfaces*, 2019, **11**, 36824–36830.
51 Z. Zhou, C. C. Bowland, M. H. Malakooti, H. Tang and H. A. Sodano, *Nanoscale*, 2016, **8**, 5098–5105.
52 Z. Zhou, H. Tang and H. A. Sodano, *Adv. Mater.*, 2014, **26**, 7547–7554.

53 H. Tang, Y. Lin, C. Andrews and H. A. Sodano, *Nanotechnology*, 2011, **22**, 015702.
54 Z. Hanani, E. H. Ablouh, S. Merselmiz, J. Ghanbaja, M. Amjoud, D. Mezzane, A. Alimoussa, M. Lahcini, M. Spreitzer, D. Vengust, M. El Marssi, I. A. Lukyanchuk, Z. Kutnjak and M. Gouné, *CrystEngComm*, 2021, **23**, 5249–5256.
55 A. Mayeen, M. S. Kala, M. S. Jayalakshmy, S. Thomas, D. Rouxel, J. Philip, R. N. Bhowmik and N. Kalarikkal, *Dalton Trans.*, 2018, **47**, 2039–2051.
56 Y. Fan, X. Huang, G. Wang and P. Jiang, *J. Phys. Chem. C*, 2015, **119**, 27330–27339.
57 Z. Hanani, E. H. Ablouh, M. Barek Amjoud, D. Mezzane, S. Fourcade and M. Gouné, *Ceram. Int.*, 2018, **44**, 10997–11000.
58 M. M. Kržmanc, H. Uršič, A. Meden, R. C. Korošec and D. Suvorov, *Ceram. Int.*, 2018, **44**, 21406–21414.
59 Z. Yang, G. Du, Z. Guo, X. Yu, Z. Chen, T. Guo and H. Liu, *J. Mater. Chem.*, 2011, **21**, 8591–8596.
60 Z. Deng, Y. Dai, W. Chen, X. Pei and J. Liao, *Nanoscale Res. Lett.*, 2010, **5**, 1217–1221.
61 Y. Zhuang, F. Li, G. Yang, Z. Xu, J. Li, B. Fu, Y. Yang and S. Zhang, *J. Am. Ceram. Soc.*, 2014, **97**, 2725–2730.
62 K. Shi, B. Chai, H. Zou, P. Shen, B. Sun, P. Jiang, Z. Shi and X. Huang, *Nano Energy*, 2021, **80**, 105515.
63 Y. Zhuang, Z. Xu, F. Li, Z. Liao and W. Liu, *RSC Adv.*, 2015, **5**, 55269–55276.
64 X. Meng, Z. Zhang, D. Lin, W. Liu, S. Zhou, S. Ge, Y. Su, C. Peng and L. Zhang, *J. Adv. Ceram.*, 2021, **10**, 991–1000.
65 L. Ye, L. Chen, J. Yu, S. Tu, B. Yan, Y. Zhao, X. Bai, Y. Gu and S. Chen, *J. Mater. Sci.: Mater. Electron.*, 2021, **32**, 3966–3978.
66 J. Yan and Y. G. Jeong, *ACS Appl. Mater. Interfaces*, 2016, **8**, 15700–15709.
67 K.-I. Park, M. Lee, Y. Liu, S. Moon, G.-T. Hwang, G. Zhu, J. E. Kim, S. O. Kim, D. K. Kim, Z. L. Wang and K. J. Lee, *Adv. Mater.*, 2012, **24**, 2937.
68 W. Qin, P. Zhou, Y. Qi and T. Zhang, *Micromachines*, 2020, **11**, 966.
69 W. Wu, L. Cheng, S. Bai, W. Dou, Q. Xu, Z. Wei and Y. Qin, *J. Mater. Chem. A*, 2013, **1**, 7332–7338.
70 Z. H. Lin, Y. Yang, J. M. Wu, Y. Liu, F. Zhang and Z. L. Wang, *J. Phys. Chem. Lett.*, 2012, **3**, 3599–3604.
71 J. H. Jung, C. Y. Chen, B. K. Yun, N. Lee, Y. Zhou, W. Jo, L. J. Chou and Z. L. Wang, *Nanotechnology*, 2012, **23**, 375401.
72 F. Bernard, L. Gimeno, B. Viala, B. Gusarov and O. Cugat, *Proceedings*, 2017, **1**, 335.
73 C. Zhao, J. Zhang, Z. L. Wang and K. Ren, *Adv. Sustainable Syst.*, 2017, **1**, 1700068.
74 G. Zhang, Q. Liao, Z. Zhang, Q. Liang, Y. Zhao, X. Zheng and Y. Zhang, *Adv. Sci.*, 2015, **3**, 1500257.
75 C. K. Jeong, C. Baek, A. I. Kingon, K. Il Park and S. H. Kim, *Small*, 2018, **14**, 1704022.
76 H. J. Oh, D. K. Kim, Y. C. Choi, S. J. Lim, J. B. Jeong, J. H. Ko, W. G. Hahm, S. W. Kim, Y. Lee, H. Kim and B. J. Yeang, *Sci. Rep.*, 2020, **10**, 16339.
77 X. Lu, H. Qu and M. Skorobogatiy, *Sci. Rep.*, 2017, **7**, 2907.
78 J. Briscoe, N. Jalali, P. Woolliams, M. Stewart, P. M. Weaver, M. Cain and S. Dunn, *Energy Environ. Sci.*, 2013, **6**, 3035–3045.
79 N. A. Hoque, P. Thakur, P. Biswas, M. M. Saikh, S. Roy, B. Bagchi, S. Das and P. P. Ray, *J. Mater. Chem. A*, 2018, **6**, 13848–13858.